Available online at www.sciencedirect.com

SciVerse ScienceDirect

Ceramics International 38 (2012) 3403–3409

CERAMICS INTERNATIONAL

www.elsevier.com/locate/ceramint

Subsolidus formation and impedance spectroscopy studies of materials in the $(Bi_2O_3)_{1-x}$ $(Y_2O_3)_x$ binary system

M.Y. Tan [a], K.B. Tan [a,*], Z. Zainal [a], C.C. Khaw [b], S.K. Chen [c]

[a] Chemistry Department, Faculty of Science, Universiti Putra Malaysia, 43400 Serdang, Selangor, Malaysia
[b] Department of Engineering, Faculty of Engineering and Science, 53300 Universiti Tunku Abdul Rahman, Malaysia
[c] Physics Department, Faculty of Science, Universiti Putra Malaysia, 43400 Serdang, Selangor, Malaysia

Received 31 October 2011; received in revised form 19 December 2011; accepted 19 December 2011
Available online 27 December 2011

Abstract

Single phase $(Bi_2O_3)_{1-x}(Y_2O_3)_x$ samples with $x = 0.15, 0.20, 0.30$ and 0.40 were successfully synthesised via conventional solid state method at the firing temperature of 800 °C over 24 h. These samples crystallised in cubic fluorite structure, space group, Fm-3m and lattice parameters, a ranging from 5.5167 Å to 5.4369 Å with an increase of doped Y_2O_3. The linear-plot obeyed Vegard's law, revealing a well-behaved substitutional solid solution existed within the incorporated dopant concentration range. $(Bi_2O_3)_{1-x}(Y_2O_3)_x$ subsolidus system was thermally stable as no phase transition or weight loss was discernable within the studied temperature. The electrical properties of the prepared samples were characterised by AC impedance analyser, HP4192 at temperature ranging from 25 °C to 850 °C in the frequency range of 5 Hz to 13 MHz. The impedance data could be represented by different RC equivalent circuits. The conduction mechanism involved two processes with different activation energies at low and high temperature regions, e.g. 1.09–1.12 eV and 0.41–0.44 eV, respectively. The ionic conductivities of the prepared samples were found decreased with increase of yttrium content. These values were in general higher than that of commercial yttria- stabilised zirconia (YSZ) solid electrolyte over wide range of temperatures.

Keywords: AC impedance spectroscopy; Solid electrolyte; Subsolidus and fluorite

1. Introduction

The demands for clean and renewable energy have stemmed from the depletion of fossil fuels and polluting by-products from conventional energy generation methods. Environmental issues, e.g. air pollution, ozone depletion, global climate change and emission of radioactive, need to be addressed carefully and sorted out in due manner. Alternative energy is considered as an effective way to harvest or convert energy from one form to another. The applications of solid electrolyte using advanced functional materials have received tremendous research interest in recent years. Ceramic oxides, such as yttria-stabilised zirconia (or YSZ), have been used as electrolyte together with composite powder mixtures, e.g. nickel oxide, NiO as anode materials in solid oxide fuel cell (SOFC). Such device converts the chemical energy of fuels directly into electricity and heat by electrochemically combining the fuel and an oxidant gas via an ion-conducting electrolyte [1–4].

This scientific breakthrough has shed new light in research particularly for materials exhibiting high ionic conductivity behaviour. The conduction mechanism is believed to be closely associated with the structural defect, vacancy and dynamic disorder within the host structure. In general, the mobile charge carriers, e.g. oxide ion, O^{2-} or Li^+, are responsible for the conduction. The structure has partial occupancy for charge carriers and the charge carriers can move from one site to another with relatively low activation energy, typically in the range of 0.1–0.9 eV [4]. Usually, only negligible electronic transport is found in solid electrolytes but then they are considered as mixed conductors if significant electronic conduction occurs favourably.

One of the promising candidates in solid electrolytes is bismuth based materials. δ-Bi_2O_3 is the most interesting phase because it exhibits the highest conductivity, 1 S cm^{-1} at 650 °C. The high ionic conductivity is due to the high intrinsic oxygen vacancy concentration and high anion mobility within

* Corresponding author. Tel.: +60 3 89467491; fax: +60 3 89435380.
E-mail address: tankb@science.upm.edu.my (K.B. Tan).

0272-8842/$36.00.
doi:10.1016/j.ceramint.2011.12.052

the structure [2,4–7]. Although different structural models are proposed by different research groups [8,9], it is generally accepted as an anion deficient fluorite structure in which bismuth, Bi, occupies face centred cubic sites. Model reported by Gattow may be viewed as time- or space-averaged occupancy of each site since oxide ions in the oxygen lattice sites could move from site to site through the bismuth sublattice [8]. The δ-Bi_2O_3 phase cannot be quenched directly to room temperature and maintained the high conductivity as at the high temperature. However, δ-Bi_2O_3 phase could be stabilised by doping pure Bi_2O_3 with appropriate amount of rare earth metal such as yttrium oxide, Y_2O_3.

In order to minimise trapping effect and subsequently maintain high conductivity of δ-Bi_2O_3, the metal cations with tri-valent, +3 had to be doped. Most of the Bi_2O_3–M_2O_3 (where M = rare earth metal) were based on either the face centred cubic δ-Bi_2O_3 form or the rhombohedral structures [9]. Datta and Meehan reported that $BiYO_3$ and subsolidus solution existed in the Bi_2O_3–Y_2O_3 binary system [10]. This cubic face centred structure was thermally stable having similar defect fluorite-type to that of δ-Bi_2O_3. Since $BiYO_3$ was structurally related to δ-Bi_2O_3, it was therefore regarded as δ^* phase. Chemical doping of Y_2O_3 was effective and successful as this dopant not only stabilised the fluorite structure, but also created oxide ion vacancies in order to preserve charge neutrality [11]. Similar study was performed by Ekhelikar and Bichile and they confirmed the solid solution limit, i.e. $0.10 \leq x \leq 0.40$ in the $(Bi_2O_3)_{1-x}(Y_2O_3)_x$ system [12]. As confirmed by X-ray analysis, all samples were phase pure and the lattice parameters were found decreased with increasing Y_2O_3 content. On the other hand, Kruidhof et al. had investigated the thermochemical stability of yttria stabilised δ-Bi_2O_3 solid solution containing 22.0–32.5% of Y_2O_3 [13]. The structure was confirmed as face centered cubic structure, stable and their electrical conductivities decreased with increasing content of Y_2O_3 [13,14].

In this paper, we focus our study on the subsolidus formation and electrical properties of materials in the $(Bi_2O_3)_{1-x}(Y_2O_3)_x$ binary system in particularly to characterise the different regions of electrical behaviour in these materials using AC impedance spectroscopy technique. The gathered information serves to provide further insight into the structure-composition-property correlation and enables one to compare the results of this subsolidus system over the literature.

2. Experimental

Samples of $(Bi_2O_3)_{1-x}(Y_2O_3)_x$ system were prepared by Bi_2O_3 (99%, Aldrich) and Y_2O_3 (99% Aldrich) as the starting materials via conventional solid state reaction. Prior to weighing, Bi_2O_3 was preheated at 300 °C for 2 h, while Y_2O_3 was preheated at 600 °C for 2 h in order to remove any moisture and impurities in the materials. Oxides were weighed out in stoichiometric quantities and the mixture was then ground homogeneously in an agate mortar with sufficient amount of acetone. The mixture was transferred into an gold boat and fired at temperature 300 °C and 600 °C for 2 h, respectively prior to final sintering at 800 °C for 24 h in furnace. Intermediate grinding was performed at 300 °C and 600 °C and final sample weight loss of material was checked. The sample was rapid cooled in air, reground and examined by Shidmazu X-ray powder diffractometer (XRD) 6000, which was equipped with a diffracted beam graphite monochromator, CuKα radiation, 1.5406 Å at a scan rate of 0.1°/min. Elemental analyses were performed by inductively coupled plasma-optical emission spectroscopy (ICP-OES) model Perkin Elmer Optima 2000 DV and Shimadzu X-ray fluorescent spectroscopy (XRF) instrument model EDX-720, respectively. Thermal stability of the phase pure samples was studied by Perkin Elmer thermal gravimetry analyser (TGA 7). Pellets of phase pure sample were prepared in 8 mm diameter and then sintered at 800 °C. The gold coated pellet was attached to two ends of conductivity jig, characterised using HP 4192A impedance spectroscopy analyser over a frequency range of 5 Hz–13 MHz. The measurements were taken from temperature 28–800 °C by incremental steps of 25 °C and/or 50 °C on a heating cycle with 30 min equilibration time. The samples were left overnight at 800 °C and a cooling cycle performed on the next day.

3. Results and discussions

3.1. Phase formation of $(Bi_2O_3)_{1-x}(Y_2O_3)_x$ solid solution

Samples with a general formula of $(Bi_2O_3)_{1-x}(Y_2O_3)_x$, where $x = 0.10$–0.45, have been synthesised by conventional solid state method. The formation of single phase samples is confirmed by the absence of characteristic XRD lines of the constituent oxides and other phases in the XRD diffraction spectra (Fig. 1). It is found that $Bi_{1-x}Y_xO_{1.5}$ solid solution, where $x = 0.15$, 0.20, 0.30, 0.35 and 0.40 crystallised in face centred cubic with lattice parameters, $5.5167\ (3) < a < 5.4462\ (6)$ Å with space group Fm-3m. Samples, $(Bi_2O_3)_{1-x}(Y_2O_3)_x$ with $x \leq 0.10$ and $x \geq 0.45$, show secondary phases due to small amount of unreacted constituent oxides, Bi_2O_3 and Y_2O_3.

The determined $(Bi_2O_3)_{1-x}(Y_2O_3)_x$ solid solution limit, i.e. $0.15 \leq x \leq 0.40$ is in good agreement as reported in the literature [12]. The formation of $(Bi_2O_3)_{1-x}(Y_2O_3)_x$ solid solution meets the necessary requirements [6,7,12–16]. Firstly, the trivalent yttrium, Y^{3+} ions that are introduced to the parent structure of Bi_2O_3 have the same charge as the Bi^{3+}. Thus, there is no other structural changes involving interstitials or vacancies would be required to maintain electroneutrality. Secondly, the percentage difference in cationic radii of Y^{3+} that replaces cations Bi^{3+} is less than 15%. The reported cationic radii of Y^{3+} and Bi^{3+} are 0.90 and 1.03 Å, respectively [17]. Lastly, the formation of solid solutions is thermodynamically stable. However, at $x = 0.45$, there are five unindexed peaks at $2\theta = 27.90°$, 28.84°, 33.18°, 48.21° and 56.80° (Fig. 1). The first, fourth and fifth peaks are corresponded to residual or unreacted δ-Bi_2O_3 (ICDD card number: 074-1373), the second peak is attributed to Y_2O_3 (ICDD card number: 044-0399) and the third peak is due to unreacted α-Bi_2O_3 (ICDD card number: 041-1449). Hence, the required condition to synthesise single phase $(Bi_2O_3)_{1-x}(Y_2O_3)_x$ solid solution using conventional

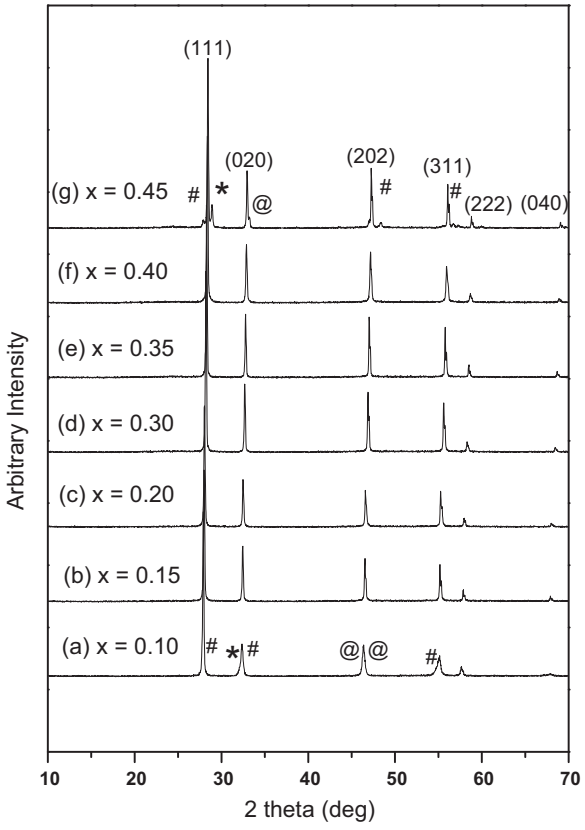

Fig. 1. XRD patterns of prepared $(Bi_2O_3)_{1-x}(Y_2O_3)_x$ samples in the range of $0.10 \leq x \leq 0.45$. *Y_2O_3, @α-Bi_2O_3 and #Bi_2O_3.

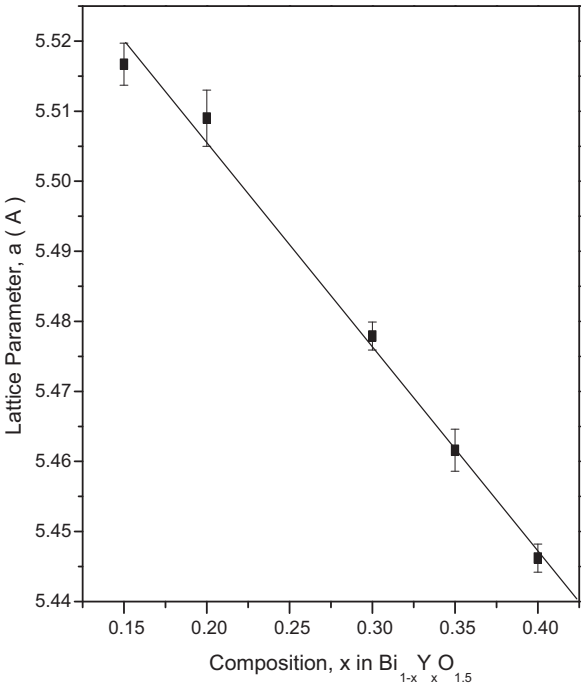

Fig. 2. Variation of lattice parameters, a against composition, x in $(Bi_2O_3)_{1-x}(Y_2O_3)_x$ solid solution.

solid state method is confirmed at the firing temperature of 800 °C over 24 h.

The lattice parameters of $(Bi_2O_3)_{1-x}(Y_2O_3)_x$ solid solution ($0.15 \leq x \leq 0.45$) are obtained from structural refinement using *Chekcell* program. The change of lattice parameter versus composition, x is plotted as shown in Fig. 2. It is observed that the lattice parameters decrease with increasing concentration of Y_2O_3 for which Vegard's law is obeyed. Since a linear relationship between the lattice parameters and concentrations of Y_2O_3 is observed, therefore the solid solution limit is confirmed as $0.15 \leq x \leq 0.40$. The shrinkage in unit cell, i.e. smaller lattice parameter with higher doped amount of Y_2O_3 could be attributed to the relatively smaller Y^{3+} cation radius. The bond length of Y–O is thus expected to be shorter than that of Bi–O and therefore substituted Y_2O_3 into Bi_2O_3 structure could have led to an overall contraction of cell parameters.

Table 1
ICP-OES elemental analysis of bismuth and yttrium in $(Bi_2O_3)_{1-x}(Y_2O_3)_x$ solid solution.

Sample	Element	Atomic percentage (%)		Experimental stoichiometric formula
		Calculated	Experimental	
$Bi_{0.60}Y_{0.40}O_{1.5}$	Bi	67.80	68.09 ± 0.89	$Bi_{0.61}Y_{0.39}O_{1.53}$
	Y	19.23	18.58 ± 0.17	
	O	12.98	13.33	
$Bi_{0.70}Y_{0.30}O_{1.5}$	Bi	74.27	72.52 ± 0.94	$Bi_{0.64}Y_{0.32}O_{1.55}$
	Y	13.54	14.22 ± 0.11	
	O	12.19	13.26	
$Bi_{0.80}Y_{0.20}O_{1.5}$	Bi	80.00	78.49 ± 0.47	$Bi_{0.73}Y_{0.20}O_{1.59}$
	Y	8.51	8.51 ± 0.04	
	O	11.48	13.00	
$Bi_{0.85}Y_{0.15}O_{1.5}$	Bi	82.63	81.27 ± 0.17	$Bi_{0.78}Y_{0.15}O_{1.57}$
	Y	6.20	6.20 ± 0.10	
	O	11.17	12.54	

3.2. Elemental analyses and thermal analysis

The ICP-OES results for $(Bi_2O_3)_{1-x}(Y_2O_3)_x$ solid solution ($0.15 \leq x \leq 0.40$) are summarised in Table 1. The elemental compositions of bismuth and yttrium determined experimentally are in good agreement with the theoretical values. The experimental sample stoichiometries are close to the expected stoichiometric formulae, confirming that there is no significant bismuth loss and considerable amount of yttrium has been successfully doped.

The experimental and expected weight percentages of Bi_2O_3 and Y_2O_3 by XRF analysis are tabulated in Table 2. There are

Table 2
Calculated and experimental XRF weight percentages of Bi_2O_3 and Y_2O_3 in $Bi_{1-x}Y_xO_{1.5}$ solid solution.

Sample	Weight percentage of Bi_2O_3 (wt%)		Weight Percentage of Y_2O_3 (wt%)	
	Calculated	Experimental	Calculated	Experimental
$Bi_{0.85}Y_{0.15}O_{1.5}$	92.12	91.36	7.88	8.24
$Bi_{0.80}Y_{0.20}O_{1.5}$	89.19	83.67	10.81	13.67
$Bi_{0.70}Y_{0.30}O_{1.5}$	82.80	76.70	17.20	21.31
$Bi_{0.60}Y_{0.40}O_{1.5}$	75.58	69.41	24.42	28.61

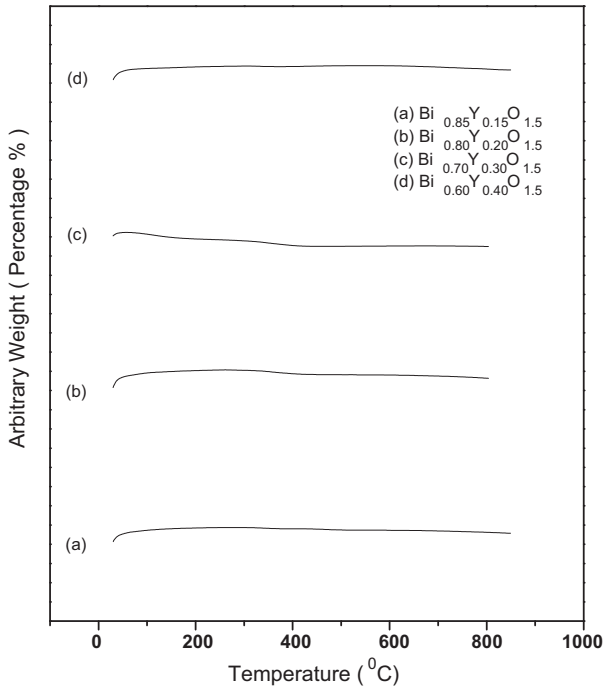

Fig. 3. Combined TGA thermograms of $(Bi_2O_3)_{1-x}(Y_2O_3)_x$ solid solution.

differences between the calculated and experimental weight percentages for each sample. Typically, experimental weight percentages of Bi_2O_3 are lower than calculated weight percentages, whereas the experimental weight percentages of Y_2O_3 are higher than calculated weight percentages. The obtained results are slightly deviated from the ICP-OES results. However, it does provide a good indication of the doped Y_2O_3 within the fluorite structure. On the other hand, the TGA thermograms of $(Bi_2O_3)_{1-x}(Y_2O_3)_x$ solid solution are combined and shown in Fig. 3. Horizontal lines across the heating temperature range are observed in all the samples, showing no any systematic weight change occurred when the samples are heated up to 900 °C.

3.3. Impedance and ionic conductivity analysis

Conductivity measurements of $(Bi_2O_3)_{1-x}(Y_2O_3)_x$ solid solution ($0.15 \leq x \leq 0.40$) are carried out from room temperature to 850 °C in heat–cool cycle. Conductivity values of these materials are extracted from high intercepts of complex plane plots (Fig. 4). Generally, complex plane plots of these materials at low temperatures, typically 250 °C to 300 °C, show a perfect semicircle at high frequency which corresponds to bulk response. As temperature increases, the semicircle becomes smaller and shifts towards lower impedance, Z' values, indicating that the property of bulk resistance of material is decreased. Above 350 °C, a spike at the lower frequency region caused by electrode effects becomes more pronounced as temperature increases. Samples within $(Bi_2O_3)_{1-x}(Y_2O_3)_x$ solid solution show similar electrical response and composition $Bi_{0.80}Y_{0.20}O_{1.5}$ ($x = 0.2$) is chosen for further discussion due to its relatively higher conductivity.

The complex plane plot of $Bi_{0.80}Y_{0.20}O_{1.5}$ shows a perfect semicircle at temperature 251 °C (Fig. 4a). The bulk or grain resistance, R_g of $Bi_{0.80}Y_{0.20}O_{1.5}$ determined by *ZView 2* program is 1.65×10^5 ohm cm. An associated capacitance of 5.17×10^{-12} F cm^{-1} is calculated at the maximum of the semicircle by the relation $\omega_{max}RC = 1$. This value falls in the pF range and therefore is attributed to bulk microstructure within the material [18,19]. The impedance data could be represented by the equivalent circuit shown in the inset of Fig. 4a and b, which contains R and C elements of the bulk material in parallel. The bulk conductivities of $Bi_{0.80}Y_{0.20}O_{1.5}$ increase with increasing temperature. The ionic or electronic conduction is easier since charge carriers have greater thermal energy, better mobility and probably higher defect concentrations at higher temperatures. It is worth nothing that the conductivities of $Bi_{0.80}Y_{0.20}O_{1.5}$ are significantly greater than $(ZrO_2)_{0.91}(Y_2O_3)_{0.09}$, a commercial applied material at different corresponding temperatures (Table 3). The operating temperatures of yttria stabilised zirconia are typically in the range of 500–800 °C for SOFC applications.

At 300 °C, there is a semicircle at high frequency corresponding to bulk resistance and a spike with 45° at the low frequency region that resulted from electrode effects (Fig. 4). The high frequency semicircle has an associated capacitance of 4.92×10^{-12} F cm^{-1}, which is typical response of bulk component. The spike has an associated capacitance of $\sim 10^{-9}$ and this is due to the formation of electrode double layer capacitance, C_{dl} at electrode electrolyte interface due to migration of ions at low frequency [18]. It is a characteristic of the behaviour of ionically conducting solids with blocking electrodes. As the degree of the spike with Z' axis is 45°, this indicates that the electrode electrolyte interface is not fully blocked by the ions. The conducting ions in the compound are oxide ions, O^{2-}, and the electrode electrolyte interface is semi-blocked by the air gap formed by the reduction of O^{2-} within the compound. As temperature increases, the electrical response due to bulk microstructure gradually diminishes and replaces by spike (Fig. 4c and d). The spike becomes more predominant above 450 °C. It is a characteristic of ionic polarisation phenomena occurs at the blocking electrodes and a diffusion limited Warburg impedance. Thus, these spikes support that the conduction of this material is arising from oxide ion conduction [19].

For an ideal Debye response representing homogeneous bulk properties, the frequency maxima of complex impedance, Z'', and electric modulus M'' peaks in the spectroscopic plots should be coincident and the full width at half maximum (FWHM) should be 1.14 decades. Fig. 5 shows that the frequency maxima of Z'' and M'' are not coincident perfectly for $Bi_{0.80}Y_{0.20}O_{1.5}$ at 251 °C. The magnitude of FWHM of the M'' peaks of $Bi_{0.80}Y_{0.20}O_{1.5}$ is approximately 1.6 decade, which deviates from that of perfect Debye. This indicates that the measured conductivity is not electrically homogeneous.

Basically, $(Bi_2O_3)_{1-x}(Y_2O_3)_x$ solid solution ($0.15 \leq x \leq 0.40$) shows reproducible conductivities in heat–cool cycle. Fig. 6 shows the Arrhenius conductivity plots for $Bi_{0.80}Y_{0.20}O_{1.5}$ sample. The ionic conductivity data for the heat–cool cycles are reversible,

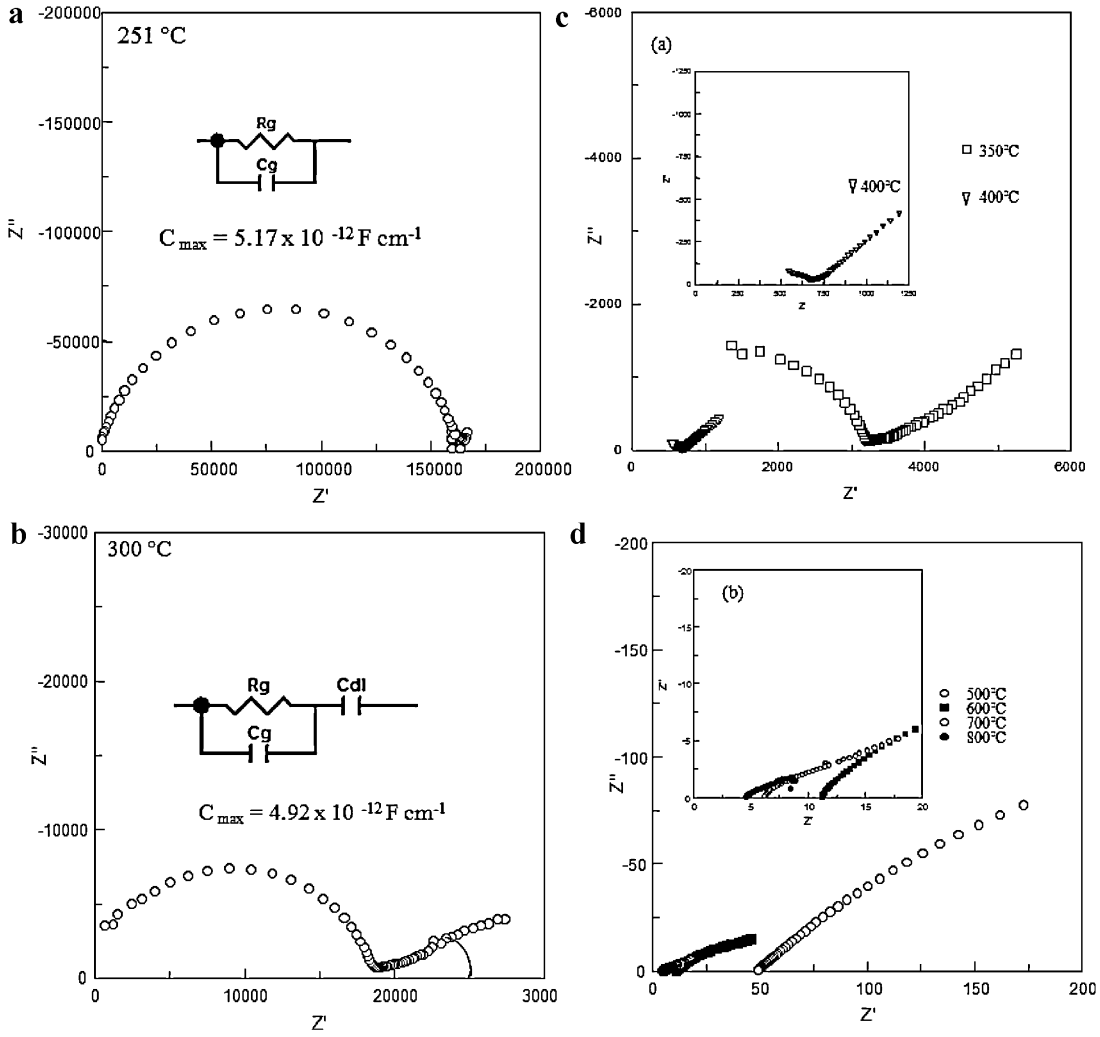

Fig. 4. Complex impedance plane plots of $Bi_{0.80}Y_{0.20}O_{1.5}$ at different temperatures: (a) 251 °C, (b) 300 °C, (c) 350–400 °C and (d) 500–800 °C.

thus the mechanisms of ionic conduction are reproducible. A distinct curvature arises from the difference in activation energies at lower and higher temperature ranges, as observed in the Arrhenius conductivity plots. This indicates that two temperature dependent activation processes are involved in the oxide ion conduction [19,20]. A change of slope from 1.11 eV to 0.44 eV at around 550 °C could be seen from cooling cycle of $Bi_{0.80}Y_{0.20}O_{1.5}$. For comparison of ionic conductivities with increasing concentration of dopant, Y_2O_3, the Arrhenius conductivity plots at second cooling cycle of $(Bi_2O_3)_{1-x}(Y_2O_3)_x$ solid solution ($0.15 \leq x \leq 0.40$) are combined and shown in Fig. 7. The ionic conductivities of $Bi_{1-x}Y_xO_{1.5}$ solid solution are observed decrease with higher x values. In other word, the ionic conductivities of $(Bi_2O_3)_{1-x}(Y_2O_3)_x$ solid solution drop with lower Bi content. As discussed earlier, the unit cells contract as the larger cationic

Table 3
Comparison of ionic conductivities of solid electrolyte $(ZrO_2)_{0.91}(Y_2O_3)_{0.09}$ and $Bi_{0.80}Y_{0.20}O_{1.5}$ at temperatures 500 and 650 °C.

Temperature (°C)	Conductivity (S cm^{-1})	
	$(ZrO_2)_{0.91}(Y_2O_3)_{0.09}$	$Bi_{0.80}Y_{0.20}O_{1.5}$
500	4.6×10^{-4}	2.01×10^{-2}
650	3.8×10^{-3}	1.18×10^{-1}

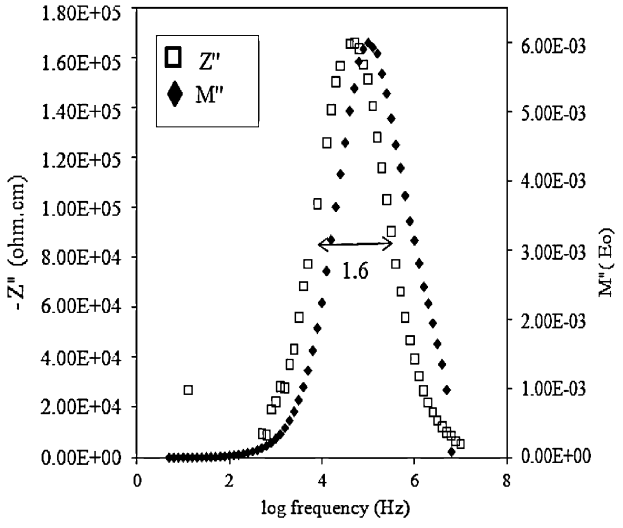

Fig. 5. Combined Z'' and M'' spectroscopic plot of $Bi_{0.80}Y_{0.20}O_{1.5}$ at 251 °C.

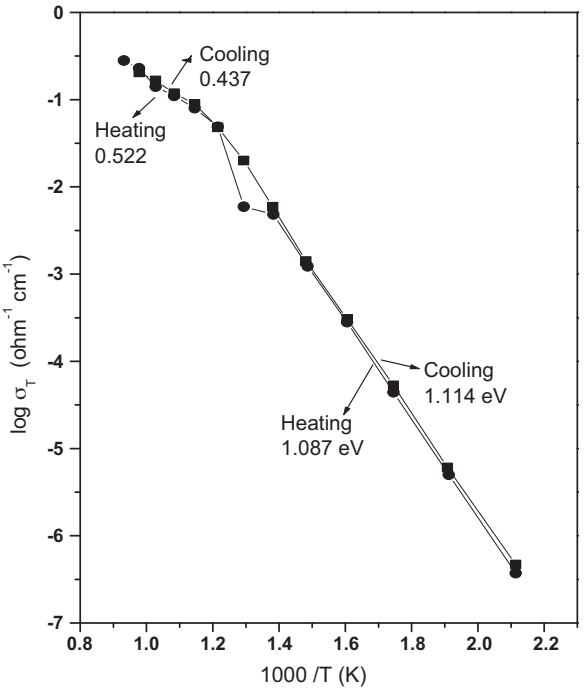

Fig. 6. Arrhenius conductivity plots of $Bi_{0.80}Y_{0.20}O_{1.5}$ for heat–cool cycles.

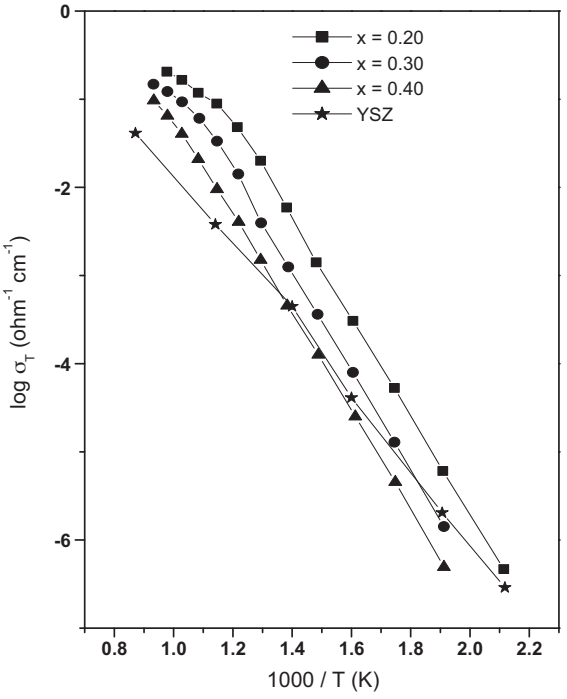

Fig. 7. Arrhenius conductivity plots of $Bi_{1-x}Y_xO_{1.5}$ ($0.40 \leq x \leq 0.20$) and yttria-stabilised zirconia, YSZ.

radius, Bi^{3+} is replaced by smaller cationic radius, Y^{3+}. The contraction of unit cell, i.e. higher Bi concentration, may restrict the partially filled oxide ions hop into adjacent oxide ion vacancies and consequently the ionic conductivities of $(Bi_2O_3)_{1-x}(Y_2O_3)_x$ solid solution are reduced. Meanwhile, the ionic conductivities of yttria-stabilised zirconia, YSZ, which is commercially used as solid electrolyte in SOFC, are included for comparison. Ionic conductivities of $Bi_{0.60}Y_{0.40}O_{1.5}$ and $Bi_{0.70}Y_{0.30}O_{1.5}$ at temperatures above 450 °C and 300 °C are somewhat higher than that of YSZ. The ionic conductivities of $Bi_{0.80}Y_{0.20}O_{1.5}$ are generally higher than that of YSZ within the temperature range 200–800 °C. Since $Bi_{0.80}Y_{0.20}O_{1.5}$ is thermally stable and exhibits higher ionic conductivity than YSZ, thus it could be therefore considered as an alternative for YSZ in industry.

3.4. Conclusion

Substitutional solid solution $(Bi_2O_3)_{1-x}(Y_2O_3)_x$ was confirmed at $0.15 \leq x \leq 0.40$ together with a decrease of lattice parameters with higher Y_2O_3 content. The cell contraction was attributed to the replacement of larger Bi^{3+} cation with smaller Y^{3+} cation. Incorporation of yttrium dopant into fluorite structured subsolidus system was ascertained by elemental analyses for which the calculated and theoretical values are highly co-related. Blocking electrodes effect was discernable as the degree of the spike with *Z*' axis obtained was 45°, showing that the electrode electrolyte interface was not fully blocked by the ions. The conducting ions in the compound were oxide ions, O^{2-}, and the electrode electrolyte interface was semi-blocked by the air gap formed by the reduction of O^{2-} within the compound. High oxide ionic conductivities were observed for all yttrium doped samples over wide range of temperatures. Distinct curvatures in Arrhenius conductivity plots were resulted from the difference in activation energies at low and high temperature regions. This indicated that two temperature dependent activation processes were involved in the conduction mechanism.

Acknowledgement

Financial support from Ministry of Higher education, Malaysia via Fundamental Research Grant Scheme (FRGS) is gratefully appreciated.

References

[1] S. Singhal, Advances in solid oxide fuel cell technology, Solid State Ionics 135 (2000) 305–313.
[2] O. Yamamoto, Solid oxide fuel cells: fundamental aspects and prospects, Electrochim. Acta 45 (2000) 2423–2435.
[3] A.B. Stambouli, E. Traversa, Solid oxide fuel cells (SOFCs): a review of an environmentally clean and efficient source of energy, Renew. Sust. Energ. Rev. 6 (2002) 433–455.
[4] A.R. West, Crystal defects, non-stoichiometry and solid solutions, in: A.R. West (Ed.), Basic Solid State Chemistry, John Wiley & Sons Ltd., New York, 1999, pp. 226–240.
[5] E.D. Wachsman, Effect of oxygen sublattice order on conductivity in highly defective fluorite oxides, J. Eur. Ceram. Soc. 24 (2004) 1281–1285.
[6] A. Watanabe, Phase equlibria in the system Bi_2O_3–Y_2O_3: no possibility of δ-Bi_2O_3 stabilization, Solid State Ionics 86–88 (1996) 1427–1430.
[7] A. Watanabe, T. Kikuchi, Cubic hexagonal of yttria-stabilized δ-bismuth sesquioxide, $Bi_{2-2x}Y_{2x}O_3$ (x = 0.215–0.235), Solid State Ionics 21 (1986) 287–291.
[8] G. Gattow, H. Schröder, About bismuth III: the crystal structure of the high-temperature modification of bismuth (III) oxide (δ-Bi_2O_3), Z. Anorg. Allg. Chem. 318 (1962) 176–189.

[9] N. Sammes, G. Tompsett, H. Näfe, F. Aldinger, Bismuth based oxide electrolytes – Structure and ionic conductivity, J. Eur. Ceram. Soc. 19 (1999) 1801–1826.
[10] R.K. Datta, J. Meehan, The system Bi_2O_3–R_2O_3 (R = Y, Gd), Z. Anorg. Allg. Chem. 383 (1971) 328–337.
[11] E. Wachsman, G. Ball, N. Jiang, D. Stevenson, Structural and defect studies in solid oxide, Solid State Ionics 52 (1992) 213–218.
[12] S. Ekhelikar, G. Bichile, Synthesis and characterization of $(Bi_2O_3)_{1-x}(Y_2O_3)_x$ and $(Bi_2O_3)_{-x}(Gd_2O_3)_x$ solid solutions, Bull. Mater. Sci. 27 (2004) 19–22.
[13] H. Kruidhof, K.D. Vries, A. Burggraaf, Thermochemical stability and nonstoichiometry of stabilized bismuth oxide solid solutions, Solid State Ionics 37 (1990) 213–215.
[14] M. Verkerk, A. Burggraaf, High oxygen ion conduction in sintered oxides of the Bi_2O_3 system, Solid State Ionics 3–4 (1981) 463–467.
[15] T. Takahashi, H. Iwahara, T. Arao, High oxide ion conduction in sintered oxides of the Bi_2O_3–Y_2O_3, J. Appl. Electrochem. 5 (1975) 187–195.
[16] T. Takahashi, H. Iwahara, Oxide ion conductors based on bismuthsesquioxide, Mater. Res. 13 (1978) 1447–1453.
[17] R.D. Shannon, Revised effective ionic radii and systematic studies of interatomic distances halides and chalcogenides, Acta Crystallogr. A 32 (1976) 751–767.
[18] D.C. Sinclair, F.B. Morrison, A.R. West, Applications of combined impedance and electric spectroscopy to characterise electroceramics, Ceram. Int. 2 (2000) 33–38.
[19] J.T.S. Irvine, D.C. Sinclair, A.R. West, Electroceramics: characterization by impedance, Adv. Mater. 2 (1990) 132–138.
[20] R. Chiba, T. Ishii, F. Yoshimura, Temperature dependence of ionic conductivity in $(1-x)Zr_{2-(x-y)}Sc_2O_{3-y}Yb_2O_3$ electrolyte material, Solid State Ionics 91 (1996) 249–256.